



Performance Comparison of Contemporary Anomaly Detectors for Detecting Man-Made Objects in Hyperspectral Images

SAFA KHAZAI, ABDOLREZA SAFARI, BARAT MOJARADI & SAEID HOMAYOUNI, Tehran, Iran

Keywords: anomaly detection, hyperspectral images, man-made objects

Summary: Anomaly detection (AD) is an important and challenging area in hyperspectral image analysis. Based on different approaches, numerous AD algorithms have been presented and developed throughout the literature. This paper aims to compare detection performances of contemporary AD algorithms for detecting man-made objects in hyperspectral imagery. The algorithms used in this study include the segmented based Reed-Xiaoli (RX) algorithm, the principal component analysis based RX (PCA-RX), the orthogonal subspace projection based anomaly detector (OSP-AD), the kernel PCA-RX, and the kernel based one-class support vector machines. To evaluate the performance of the algorithms, three real hyperspectral datasets are employed. The performance comparison is then carried out on the basis of the receiving operative characteristics (ROC) curve and the average of false alarm rate (AFAR). Experimental results suggest that among the AD algorithms the OSP-AD is the most promising detector for detecting man-made targets.

Zusammenfassung: Vergleich der Leistungsfähigkeit von modernen Anomaliedetektoren zur Erkennung von künstlichen Objekten in Hyperspektralbildern. Die Erkennung von Anomalien in der Analyse von Hyperspektralbildern ist eine wichtige und anspruchsvolle Aufgabe. In der Literatur findet man viele Algorithmen zur Anomaliedetektion. Dieser Artikel vergleicht die modernen Detektoren hinsichtlich ihrer Leistungsfähigkeit zur Erkennung von künstlichen Objekten. Die Studie berücksichtigt den „Segmented Based Reed-Xiaoli (RX) Algorithmus“, den auf der Hauptachsenanalyse basierenden Reed-Xiaoli (RX) Algorithmus (PCA-RX), den auf der „Orthogonal Subspace Projection“ basierenden Anomaliedetektor (OSP-AD), den Kernel PCA-RX, and die „Kernel Based One-Class Support Vector Machines“. Der Untersuchung lagen drei Hyperspektral Datensätze zu Grunde. Als Kenngrößen wurden die „Receiving Operative Characteristics (ROC) Curve“ und die „Average of False Alarm Rate (AFAR)“ gewählt. Nach unseren Ergebnissen dürfte der OSP-AD für die Erkennung von künstlichen Objekten am geeignetsten sein.

1 Introduction

Hyperspectral images in general consist of hundreds of narrow and contiguous spectral channels, from the visible to the shortwave infrared region of the electromagnetic spectrum. Such data have great potential to detect and identify earth surface objects and phenomena in a remotely sensed scene. When the signature of the target of interest is known, the target detection (TD) approach can be used. However, TD algorithms are dependent on the degree of signal mismatch between the spectral libraries and the spectra observed in an

image. This is because of the difficulties to perform an accurate spectral calibration and to get reliable atmospheric data to convert reflectance values to the radiance spectra (BANNERJEE et al. 2006). Moreover, in many applications, the spectral signatures of the targets are often unknown. Hence, the anomaly detection (AD) approach can be used as an automatic TD system (WILSON 1998). AD algorithms enable one to detect targets whose signatures are spectrally distinct from their environment with no *a priori* knowledge other than that targets are rare, i.e. they have a low probability of occurrence in an image

scene (REED & YU 1990, BANERJEE et al. 2006, SCHWEIZER & MOURA 2001).

The kind of anomalies to be detected depends on the specific application. They may vary from crop stress identification in precision agriculture and infected trees in forestry to rare minerals in geology and mining (MATTEOLI et al. 2010). In particular, man-made objects are the most common type of anomalies considered in the public safety domain, e.g. search and rescue operations, and reconnaissance and surveillance applications. Man-made objects are typically characterized by a spectral signature different from the signatures of their surroundings. Moreover, in contrast to natural anomalies, the sizes of man-made anomalies are usually known. Also, depending on the spatial resolution of the sensor, the man-made targets may not be clearly resolved; therefore, they cover only a few pixels, i.e. multipixel targets, or even less than a single pixel, i.e. subpixel targets (MATTEOLI et al. 2010).

The Reed-Xiaoli (RX) (REED & YU 1990) is a benchmark anomaly detector for hyperspectral images. It is derived from the generalized likelihood ratio test (GLRT) (KAY 1998). The RX, along with its many modified versions (CHANG 2002), requires that the covariance matrix can be estimated from the neighbourhood pixels of the target pixel, i.e. the local background. As a result, the detection performance of RX is strongly affected by two problems. The first problem is the small sample size. It requires the estimation of a local background covariance matrix from a small number of samples in the high-dimensional space. Under this circumstance, the result is a badly-conditioned and unstable estimation. The second problem is the non-homogeneity of the local background; if this occurs, the effectiveness of the covariance matrix estimation is undetermined (MATTEOLI et al. 2009).

To overcome the problems with RX, numerous algorithms based on different AD approaches have been presented and developed in the literature. The main difference between the AD approaches lies in the manner in which the background is characterized. In previous studies, no comparative analysis of the contemporary AD algorithms performed on the same dataset and also in identical operat-

ing conditions has been done. This study aims to provide such a comparative analysis for the detection of man-made objects. The detection performance of the AD algorithms is generally evaluated on either multipixel or sometimes only on subpixel targets. In contrast, this research attempts to provide a quantitative evaluation of the AD methods at both multipixel and subpixel levels.

The rest of this paper is organized as follows. Section 2 provides an overview of the AD approaches. Materials and methods are given in section 3. Experimental results and discussions are outlined and argued in sections 4 and 5, respectively. Finally, concluding remarks are given in section 6.

2 The AD Approaches

The AD approaches can be categorized into three major groups as follows.

1) Improved versions of the RX that use solutions to improve the estimation of the covariance matrix. A possible solution is to regularize the covariance matrix (HOFFBECK & LANDGREBE 1996). Based on this solution, NASRABADI (2008) proposed the regularized-RX that regularizes the covariance matrix by adding a scaled identity matrix to it. However, the most common solutions are as follows:

- Clustering-based solution. This solution models the background using a clustering of all image pixels. A well-known AD algorithm that uses this solution is the segmented based RX (Seg-RX) proposed by CARLOTTO (2005). Based on a hyperspectral dataset, MATTEOLI et al. (2007) showed that the performance of the Seg-RX is superior to the regularized-RX.
- Dimension reduction (DR) solution. This solution uses DR techniques to reduce the dimension of hyperspectral data prior to AD using RX. In fact, the principal component analysis (PCA) is the common technique used in the DR literature. Therefore, the PCA based RX (PCA-RX) (BASENER & MESSINGER 2009) can be considered as the conventional DR-based detector.

2) Linear subspace based methods. These methods use the linear mixing model to exploit the fact that target and background signals can be reasonably assumed lying in two distinct subspaces of the data space (MATTEOLI et al. 2010). Two well-known methods in this category are the signal subspace processing AD (SSP-AD) (RANNEY & SOUMEKH 2006) and the orthogonal subspace projection based AD (OSP-AD) (CHANG 2005). MATTEOLI et al. (2007) showed that the OSP-AD outperforms the SSP-AD algorithm based on a hyperspectral image, in which several target panels have been embedded.

3) Kernel-based methods. The basic principle of these methods is that a nonlinear mapping is used to extend the input space to a higher dimensional feature space, the so-called *Hilbert* space (KWON & NASRABADI 2007). Kernel functions are used to implicitly compute the dot products in *Hilbert* space without mapping the input vectors into that space (SCHÖLKOPF et al. 2001). The Gaussian kernel is commonly accepted for kernel methods (TAX 2001) given by $k(x_i, x_j) = \exp(-|x_i - x_j|^2 / \sigma^2)$, where x_i and x_j are two objects in the original feature, i.e. spectral band, space, and σ denotes the Gaussian kernel width.

The kernel-based AD methods can be grouped into two sub-categories:

- Kernel-based versions of the RX that adopt a Gaussian model in *Hilbert* feature space. The Kernel-RX (KWON & NASRABADI 2005) and the Kernel PCA-RX (KPCA-RX) (NASRABADI 2009) are two known methods in this category. NASRABADI (2009) showed that KPCA-RX outperforms the Kernel-RX on the HYDICE forest radiance dataset.
- Non-parametric methods such as the kernel-based one-class support vector machines (K1SVM) (TAX & DUIN 1999). For the first time, BANERJEE et al. (2006) used the K1SVM for AD in hyperspectral images. Based on the HYDICE forest radiance dataset, they also showed that the detection performance of the K1SVM is superior to that of the Gaussian Markov random field (GMRF) based detector proposed by SCHWEIZER & MOURA (2001).

3 Materials and Methods

3.1 Data Description

There is a lack of shared hyperspectral datasets for detection purposes (MATTEOLI et al. 2010). Moreover, the available datasets contain few target samples with known ground truth target locations for valid tests. Hence, most of previous works published, especially those about the subpixel AD, have used simulated data for evaluating the detection performance of AD algorithms.

The only available dataset, which contains several subpixel man-made objects, is the target detection blind test (TDBT) dataset (RIT 2012). Moreover, the FOI (Swedish Defense Research Agency) has provided a hyperspectral dataset containing some vehicles at multipixel level placed in a countryside where no such objects are expected. This dataset is publicly available at FOI (2012). In this study, we also employ an AVIRIS (Airborne Visible and InfraRed Imaging Spectrometer) dataset that contains some multipixel helicopters.

TDBT dataset

The TDBT dataset includes two HyMap radiance and reflectance images of Cooke City in Montana, USA. The images were collected by the airborne HyMap (Hyperspectral Mapper) sensor, which has 126 spectral bands (SNYDER et al. 2008). The ground resolution of the imagery data is approximately 3 m.

In the HyMap images twelve man-made objects were deployed in an open grass region during the airborne image acquisition. We chose ROI-1 with the size of 90×90 pixels in the HyMap radiance image which covers the entire open grass region (Fig. 1). Two



Fig. 1: True colour composite of the HyMap radiance image. The box specifies the ROI-1 on which the positions of self-test targets are superimposed.

Tab. 1: Characteristics of the targets.

Self-test targets			Blind-test targets		
Name	Size	Type	Name	Size	Type
F1	3 × 3 m	Red Cotton	F5a	2 × 2 m	Maroon Nylon
F2	3 × 3 m	Yellow Nylon	F5b	1 × 1 m	Maroon Nylon
F3a	2 × 2 m	Blue Cotton	F6a	2 × 2 m	Gray Nylon
F3b	1 × 1 m	Blue Cotton	F6b	1 × 1 m	Gray Nylon
F4a	2 × 2 m	Red Nylon	F7a	2 × 2 m <td Green Cotton	
F4b	1 × 1 m	Red Nylon	F7b	1 × 1 m	Green Cotton

of the twelve targets are at full pixel, i.e. resolved size; the other ten are at subpixel sizes. The targets include six fabric panels for the self-test and six for the blind-test. Fig. 1 shows the locations of six self-test targets in the ROI-1, while Tab. 1 briefly describes each target in more detail. In Fig. 1, the positions of blind-test targets are not known, because the (ground truth) locations of these targets are currently unavailable to users.

AVIRIS dataset

The data is an airborne hyperspectral image of a naval air station in San Diego, California, collected by AVIRIS in 1998. The image has 220 spectral bands with a 10 nm spectral

width from 0.4 to 2.45 μm and with a ground sampling distance of 3.5 m. The 20 atmospheric water absorption bands (numbered 104–108, 150–163, and 220) were removed from the original image. In addition, 11 noisy bands with low signal-to-noise ratios (numbered 103, 109–112, 148–149, 164–165, and 217–219) were removed, resulting in a total of 189 bands. From this image, a subset consists of 80×70 pixels is used, named ROI-2 (Fig. 2). The ROI-2 contains six Sea Hawk helicopters as multipixel targets. These targets have been detected by the spectral angle mapper (SAM) algorithm with an angle threshold of 0.05.

FOI dataset

This dataset was collected in an airborne measurement over a countryside in Sweden. It has 60 spectral bands in the visual and near infrared range (390 nm–960 nm) with spectral resolution about 10 nm (WADSTRÖMER et al. 2010). The dataset includes the two scenes 1 and 2 which consist of 1024×4000 pixels where for the scene 1 the ground truth of the objects of interest is known. Moreover, each scene was captured in four flights. From scene 1, we used four test subsets with the size of 45×45 pixels around four vehicles (Fig. 3).

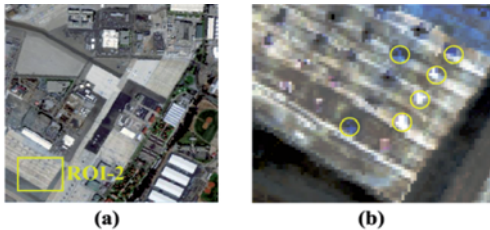


Fig. 2: (a) colour composite of the AVIRIS image; (b) zoomed window of the ROI-2 where the circles denote the helicopters.



Fig. 3: FOI dataset; left: colour composite of scene 1 (flight 4) with the test subsets around four vehicles; right: picture of some of the vehicles in scene 1.

3.2 Contemporary AD Algorithms used

Seg-RX

The Seg-RX requires that an unsupervised classification, i.e. segmentation, is performed prior to perform the RX. After obtaining a thematic map, the mean vector and the covariance matrix are estimated over each cluster. Finally, to assign an anomaly value to each test pixel y , the well-known Mahalanobis distance is computed between the y and its spectrally nearest cluster j as follows (MATTEOLI et al. 2009):

$$SRX(y) = (y - \hat{\mu}_j)^T \hat{C}_j^{-1} (y - \hat{\mu}_j) \underset{>H_1}{\overset{\leq H_0}{\eta}} \quad (1)$$

where $\hat{\mu}_j$ and \hat{C}_j are the mean spectral vector and the estimated covariance matrix for cluster j , and η is a detection threshold. The spectrally nearest cluster is typically related to the most common cluster in the local neighbouring pixels around the target pixel. The test (1) makes a decision between two competing hypotheses: H_0 (target absent hypothesis) and H_1 (target present hypothesis).

To segment the images, we employed the well-known K-means algorithm. The main problem of K-means is how to choose the optimal number of clusters. A good solution to select the optimum number of clusters is to apply the K-means algorithm with a different number of desired clusters. Then, one can select the best solution among them by a validity index such as the Davies-Bouldin index (DURAN & PETROU 2007).

PCA-RX

The PCA-RX detector is performed by applying a forward PCA transform, setting the appropriate value of the first PCs to be retained, applying an inverse PCA, and then performing the RX on the resulting image (BASENER & MESSINGER 2009). The PCA is known for its ability to map the data for finding the most important or influencing components in a dataset. These components are optimal and can almost completely represent all data in a reduced feature space. The principal components (PCs) are uncorrelated and ordered ac-

ording to their magnitude of variance of the original signal (JACKSON 1991).

By performing PCA, it can be expected that a few PCs can explain most of the variation in the original data. A key question, that arises here, is how the number of the first PCs should be chosen. There are several methods presented in the literature for determining the optimal number of PCs. A simple but efficient method is the eigenvalue ratio estimator (ERE) algorithm (AHN & HORENSTEIN 2008). It estimates the optimum number of first PCs via maximizing the ratio of two adjacent eigenvalues (in decreasing order) of the data covariance matrix.

OSP-AD

The use of OSP for AD was proposed by CHANG (2005). For target detection tasks, the OSP detector is given by

$$OSP(y) = d^T (I - WW^{\#}) y \underset{>H_1}{\overset{\leq H_0}{\eta}} \quad (2)$$

where d is a given spectral signature, $W^{\#} = (W^T W)^{-1} W^T$, and W is a matrix whose columns are projection vectors. The product $WW^{\#}$ represents a subspace for characterizing the spectra that are used to generate the projection vectors. The projection vectors are defined as either endmembers or eigenvectors obtained by the first components of the singular value decomposition (SVD) (MATTEOLI et al. 2010). However, for AD tasks, the y can be used directly to define the d . Moreover, for detecting the multipixel targets which have distinct spectra from the local background pixels, the mean spectrum of the local background pixels is used as a projection vector for local background pixels. In this regard, the resulting detector does not require determining the projection vectors by SVD.

K1SVM

Two K1SVM algorithms have been presented in the literature. The first one is called the v -support vector classifier (v -SVC) (SCHÖLKOPF et al. 1999) and aims at finding a hyperplane that separates normal training data from the origin with maximum margin. The second one is the support vector domain description

(SVDD) which is the most common K1SVM algorithm. The SVDD seeks the minimum hypersphere that encloses all normal training data (TAX & DUIN 1999). When using the Gaussian kernel, the ν -SVC solution is equivalent to that of the SVDD (TAX 2001). Given n pixels $\{x_i\}_{i=1}^n$ belonging to the local background and a Gaussian kernel k , the K1SVM problem becomes the following:

$$\min_{\alpha_i} \sum_i \sum_j \alpha_i \alpha_j k(x_i, x_j) \quad (3)$$

with two constraints on Lagrange multipliers (α_i): $\sum \alpha_i = 1$ and $0 \leq \alpha_i \leq 1/(nv)$, where objects x_i with nonzero α_i are called the support vectors (SVs), and ν is called the rejection rate which tackles the presence of outliers within the local background for constructing an optimal hypersphere.

The K1SVM test statistic defines a pixel y is an anomaly when the Euclidean distance from the y to the centre of the hypersphere is bigger than the hypersphere radius (TAX 2001).

$$1 - 2 \sum_i \alpha_i k(x_i, y) + \sum_i \sum_j \alpha_i \alpha_j k(x_i, x_j) > R^2 \quad (4)$$

where R can be determined by calculating the distance from the centre of hypersphere to any of the SVs on the boundary, i.e. objects x_i with $0 < \alpha_i < 1/(nv)$. To improve the detection performance of K1SVM in hyperspectral images, a normalized test statistic can be derived through dividing the original test statistic by the squared radius (BANERJEE et al. 2006).

The main problem of kernel-based AD methods such as the K1SVM is the optimal setting of σ . A straightforward method for estimation of the σ is given by KHAZAI et al. (2011):

$$\hat{\sigma} = \frac{d_{max}}{\sqrt{\ln(n(1-\nu)+1)}} \quad (5)$$

where d_{max} is the maximum Euclidean distance between training instances, i.e. surrounding pixels of the target pixel, and the ν is set experimentally by users. In this study, we set ν to 0.1; this means that 10% of pixels in the local background are allowed to be outliers.

KPCA-RX

The KPCA (SCHÖLKOPF et al. 1998) is an algorithm for computing the PC vectors in *Hilbert* feature space. However, the KPCA-RX (NASRABADI 2009) is an improved version of the Kernel-RX. This detector is compactly given by the following test statistic:

$$KPCA(y) = (K_y - K_{\bar{\mu}})^T W W^T (K_y - K_{\bar{\mu}}) \stackrel{\leq H_0}{> H_1} \eta \quad (6)$$

where K_y is the centred $k(y, X_b)$ which is a kernel-based vector that uses local background pixels $X_b = [x_1, x_2, \dots, x_n]$, $K_{\bar{\mu}}$ is the centred $k(\bar{x}, X_b)$ that uses $\bar{x} = 1/n \sum x_i$ as input, and W is a matrix containing the most significant, i.e. the first, eigenvectors of the centred kernel matrix $k(X_b, X_b)$. The number of first eigenvectors is a configurable constant that can be estimated using the ERE method.

3.3 Accuracy Assessment

The primary way used to analyse the ability of AD algorithms is a two-dimensional display of the detection maps. To obtain a fair visual comparison between the AD algorithms, each detection map should be normalized by its maximum value. However, the detection performance of AD methods is usually evaluated based on their experimental receiver operating characteristic (ROC) curves (WILSON 1998). The ROC curve represents the detection rate versus the false alarm rate (FAR) over a particular operating scenario. The detection values for the entire data are, firstly, normalized between zero and one. Then, the detection threshold varies from one to zero through a decrement rate, e.g. 0.001. For each detection threshold, the number of target pixels correctly detected and the corresponding number of false alarms, i.e. non-target pixels, are computed based on the ground truth data of the target pixels.

In this study, the experimental ROC curves of the AD algorithms are plotted using a log-scale on the FAR axis. Compared to the conventional scale of the FAR axis, behaviours of the detectors in a low FAR region are better demonstrated using the log-scale. It is worth-

while to note that the low FAR region is the actual operating region of interest for AD methods (MATTEOLI et al. 2010). In this study, we compare the performance of the AD algorithms in the low FAR region ranging from 0 to 0.01.

Moreover, to get a quantitative evaluation of the AD methods, the average of FAR (AFAR) values (BAJORSKI et al. 2004) is used. The AFAR is calculated by averaging the FAR encountered for each detected target pixel i as follows:

$$AFAR = \frac{1}{m} \sum_{i=1}^m FAR_i \quad (7)$$

where m represents the number of target pixels. In this study, to alleviate the problem of few target samples in the available datasets, 95% confidence intervals (assuming a Gaussian trial) for AFAR values are computed given by KEREKES (2008):

$$a \pm \frac{\sqrt{a(1-a)}\tau_{N-1,0.025}}{\sqrt{N}} \quad (8)$$

where a is the AFAR value, N represents the number of image pixels within the ROI, and $\tau_{N-1,0.025}$ denotes the cut-off value of a Student t distributed random variable with $N-1$ degrees of freedom such that the probability that the Student t random variable is greater than the cut-off value is $(1-0.95)/2$, i.e. 0.025.

4 Experimental Results

For each dataset, all pixel vectors are first normalized by a maximum spectral value in the image, so that the entries of the normalized pixel vectors fit into the interval of spectral values between zero and one. The rescaling of pixel vectors was mainly performed to effectively utilize the dynamic range of Gaussian kernel used for kernel-based methods (KWON & NASRABADI 2005).

An important decision for the AD methods is the way to choose the local background of each pixel. Generally, the dual window technique is used on multipixel targets as the size of targets of interest is bigger than the ground resolution of the image. This technique sepa-

rates the local area around each pixel into two regions, an inner window region (IWR) and an outer window region (OWR). The IWR is used to capture a target present, while the OWR is employed to model the local background of the target. For ROI-1, as the size of IWR is always 1×1 , the size of OWR should be set only. Experimentally, a constant window size of 5×5 is used to scan the image for all the algorithms on subpixel targets. For ROI-2, the sizes of IWR and OWR were experimentally selected 5×5 (as the length of helicopters is about 15 m) and 11×11 pixels, respectively. Also, for FOI subsets, we used the size of IWR and OWR to 15×15 as the length of vehicles is 7 m and $31 \text{ m} \times 31 \text{ m}$, respectively.

4.1 Results for TDBT Dataset

Fig. 4 presents the normalized detection results obtained on the ROI-1, where the positions of the self-test target pixels are superimposed.

From Fig. 4, it can be observed that while the OSP-AD provides the best background suppression ability, the K1SVM results in the worst background suppression in comparison with the other algorithms.

Fig. 5 presents the experimental ROC curves of the AD methods obtained on the ROI-1. It shows that the OSP-AD and Seg-RX result in better ROC curves compared to the other algorithms in the low FAR region considered. However, the AFAR values with 95% confidence intervals are $2\% \pm 1\%$, $4\% \pm 1\%$, $5\% \pm 1\%$, $6\% \pm 1\%$, and $7\% \pm 1\%$ using

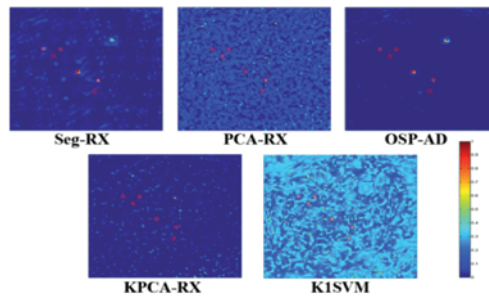


Fig. 4: 2D detection results in the ROI-2 using the AD methods. The target pixels are denoted by red circles.

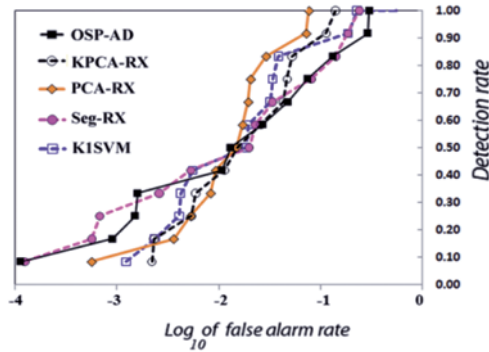


Fig. 5: Experimental ROC curves of the algorithms obtained on the ROI-1.

the PCA-RX, KPCA-RX, Seg-RX, OSP-AD, and K1SVM detectors. Therefore, the PCA-RX provides about 2%, 3%, 4%, and 5% less AFAR compared to the KPCA-RX, Seg-RX, OSP-AD, and K1SVM, respectively. Consequently, the PCA-RX manages to detect all subpixel targets with a lower AFAR to a greater degree than other algorithms.

4.2 Results for AVIRIS Dataset

Fig. 6 depicts the normalized detection results obtained on the ROI-2, where the positions of the target pixels are superimposed. Moreover, Fig. 7 shows the experimental ROC curves obtained by the AD methods.

As can be seen in Fig. 6, both the OSP-AD and PCA-RX algorithms provide strong background suppression ability in comparison with

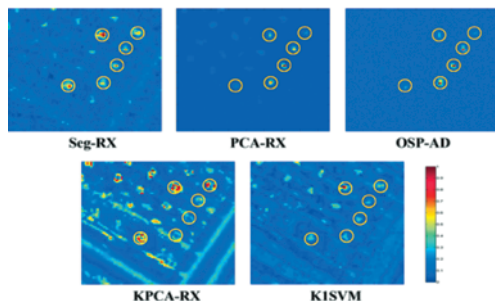


Fig. 6: 2D detection results of the AD methods obtained on the ROI-2. The target pixels are denoted by yellow circles.

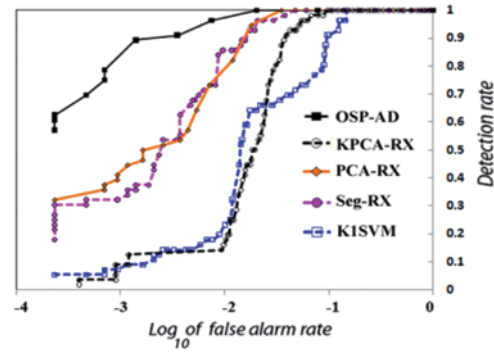


Fig. 7: Experimental ROC curves of the algorithms obtained in the ROI-2.

the other algorithms. Moreover, based on a comparison of ROC curves, Fig. 7 illustrates that the OSP-AD yields a superior detection performance compared to the other detectors in both the low and high FAR regions.

The AFAR values with 95% confidence intervals are $0.05\% \pm 0.04\%$, $0.09\% \pm 0.07\%$, $0.4\% \pm 0.1\%$, $2.1\% \pm 1\%$, and $3.2\% \pm 1\%$ using the OSP-AD, PCA-RX, Seg-RX, KPCA-RX, and K1SVM detectors. Thus, the OSP-AD decreases the AFAR value about 0.04%, 0.35%, 1.95%, 2.05%, and 3.15% compared to the PCA-RX, Seg-RX, KPCA-RX, and K1SVM, respectively. Moreover, the application of PCA-RX results in similar AFAR values exceeding OSP-AD by only 0.04%.

4.3 Results for FOI Dataset

Fig. 8 depicts the normalized detection results of the AD methods obtained on the FOI test subsets. It highlights that for background suppression, while the best results are obtained on the test subset 4, the worst results are achieved on the test subset 3.

Fig. 9 shows the average ROC curves of the AD methods achieved on the four test sets. From this figure, we can observe that the OSP-AD performs the best out of all the AD algorithms in both the low and high FAR regions. In addition, it illustrates that the PCA-RX has the lowest performance in the low FAR region. Moreover, Figs. 8 and 9 indicate that among the AD algorithms the kernel-based methods,

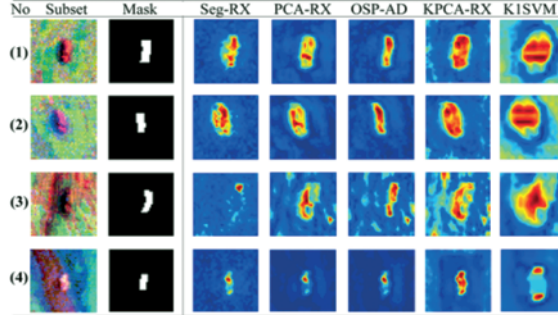


Fig. 8: FOI test subsets around each target with detection maps obtained by AD methods.

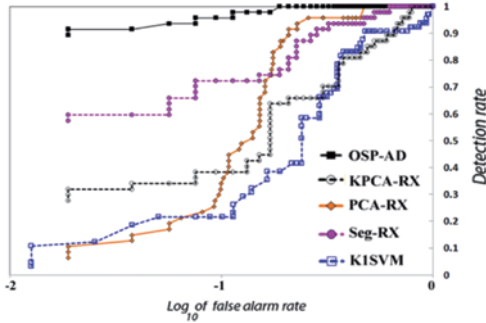


Fig. 9: Average ROC curves of the algorithms obtained on the four FOI test subsets.

i.e. K1SVM and KPCA-RX, provide the worst results on the examined test subsets.

The results also show that the AFAR values of the methods with their 95% confidence intervals are $3.2\% \pm 1\%$, $3.7\% \pm 1\%$, $4.3\% \pm 1\%$, $7.9\% \pm 1\%$, and $12\% \pm 2\%$ using the OSP-AD, PCA-RX, Seg-RX, KPCA-RX, and K1SVM algorithms, respectively. Thus, for the FOI test subsets, the OSP-AD performs the best out of all the AD algorithms considered. Comparative analysis also reveals that the PCA-RX provides only a 0.5% smaller AFAR value than the OSP-AD.

Tab. 2: ID and range of AFAR values obtained on the datasets used.

Dataset →	TDBT (ROI-1)	AVIRIS (ROI-2)	FOI (test subsets)			
			1	2	3	4
ID	2	1	34	30	29	8
The AFAR values	2%–7%	0.05%–3%	3.2%–12%			

5 Discussion

Based on the experimental results obtained using the contemporary AD algorithms, two important points are presented and discussed here:

5.1 The Effect of Background Complexity on Detection Performance

In general, when the local background consists of multiple data classes, AD algorithms suffer from low performance. A solution to evaluate the complexity level of the background is estimating the intrinsic dimensionality (ID) of the data. A simple method for estimating the ID in a given dataset is to estimate the number of first PCs to be retained (MARTINEZ et al. 2010). Based on the ERE method, Tab. 2 shows the number of ID obtained over each dataset.

From Tab. 2, we can observe that the TDBT and AVIRIS datasets have a low complexity level of background. In contrast, the complexity level of the background for the FOI test subsets is very high. However, comparing the results obtained from the AVIRIS and FOI

subsets, it can be concluded that the poor performance of the detectors on FOI test subsets is due to the high complexity level of the background. Clearly, when the value of estimated ID is not significant, AD algorithms can provide appropriate results. This can be demonstrated on the TDBT and AVIRIS datasets as the AFAR values of the methods is very low compared to the FOI test subsets.

5.2 Comparison with other Results

Based on the HYDICE forest radiance dataset, the results obtained by NASRABADI (2009) and BANERJEE et al. (2006) show that the KPCA-RX and K1SVM can detect man-made objects well. Nonetheless, our experiments demonstrate that these kernel-based AD algorithms result in poor performance compared to the OSP-AD and PCA-RX algorithms. This result implies that using the kernel-based AD methods, it may not be possible to detect man-made anomalies in the original feature space. EVANGELISTA et al. (2006) also indicated that the kernel-based AD methods suffer from the so-called curse of dimensionality. As a result, the kernel-based AD methods may provide a high detection performance in combination with DR techniques (as a preprocessing step).

On the other hand, in a study for the purpose of detecting multipixel man-made targets in hyperspectral images, BORGHYS et al. (2011) compared the detection performance of the OSP-AD and Seg-RX algorithms. They reported that the OSP-AD gives better results than the Seg-RX using three HyMap image scenes, Oberpfaffenhofen, Hartheim, and Camargue. Moreover, MATTEOLI et al. (2007) analysed an image dataset acquired by the SIM-GA sensor, and showed that the OSP-AD has superior performance compared to the Seg-RX algorithm. This study also confirms the superiority of the OSP-AD over the Seg-RX algorithm based on the experimental results obtained from the AVIRIS and FOI datasets.

6 Conclusion

The experiments in question suggest some conclusions about the capabilities of five contemporary anomaly detectors Seg-RX, PCA-RX, OSP-AD, KPCA-RX, and K1SVM in detecting man-made anomalies. Based on the three examined datasets, the results showed that the OSP-AD achieves the best performance for detecting multipixel man-made targets. Moreover, to detect the subpixel targets, while the PCA-RX is overall the best AD algorithm, the OSP-AD and Seg-RX provide the best performance in the low FAR region, which is in fact the operating region of interest for AD methods. Consequently, the OSP-AD is the most promising AD algorithm for detecting man-made objects. This research also found that the kernel-based methods applied to the data in the original space are not suitable for detecting man-made objects. However, we point out that the use of more hyperspectral datasets can provide more reliable assessments. In addition, all results are dependent on the IWR and OWR parameter settings, signal-to-noise level, and the free parameters involved. The impact of these factors on the detection performance along with the computational complexity of the algorithms will be investigated in future work.

Acknowledgements

The authors would like to thank the Digital Imaging and Remote Sensing group in the Center for Imaging Science, Rochester Institute of Technology, Rochester, NY, USA, for providing the Target Detection Test datasets, Dr. J.P. KERÉKES for his valuable help in providing truth locations of the blind-test targets, the Swedish Defence Research Agency, specially NICLAS WADSTRÖMER and JÖRGEN AHLBERG, for providing the FOI dataset, and Dr. D.M.J. TAX for the MATLAB dd-tools, which allowed us to implement the K1SVM.

References

- AHN, S.C. & HORENSTEIN, A., 2008: Eigenvalue ratio test for the number of factors. – Working paper, Arizona State University.
- BAJORSKI, P., IENTILUCCI, E. & SCHOTT, J., 2004: Comparison of basis vector selection methods for target and background subspaces as applied to subpixel target detection. – *SPIE* **5425**: 97–108.
- BANERJEE, A., BURLINA, P. & DIEHL, C., 2006: A support vector method for anomaly detection in hyperspectral imagery. – *IEEE Transactions on Geoscience and Remote Sensing* **44** (8): 2282–2291.
- BASENER, W.F. & MESSINGER, D.W., 2009: Enhanced detection and visualization of anomalies in spectral imagery. – SHEN, S.S. & LEWIS, P.E. (eds.): *Algorithms and Technologies for Multispectral, Hyperspectral, and Ultraspectral Imagery XV*. – *SPIE* **7334**.
- BORGHYS, D., ACHARD, V., ROTMAN, S.R., GORELIK, N., PERNEEL, C. & SCHWEICHER, E., 2011: Hyperspectral anomaly detection: a comparative evaluation of methods. – *General Assembly and Scientific Symposium of the International Union of Radio Science XXX URSI*: 1–4.
- CARLOTTO, M.J., 2005: A cluster-based approach for detecting man-made objects and changes in imagery. – *IEEE Transactions on Geoscience and Remote Sensing* **43** (2): 374–387.
- CHANG, C.-I., 2002: Anomaly detection and classification for hyperspectral imagery. – *IEEE Transactions on Geoscience and Remote Sensing* **40** (6): 1314–1325.
- CHANG, C.-I., 2005: Orthogonal subspace projection (OSP) revisited: A comprehensive study and analysis. – *IEEE Transactions on Geoscience and Remote Sensing* **43** (3): 502–518.
- DURAN, D. & PETROU, M., 2007: A time-efficient method for anomaly detection in hyperspectral images. – *IEEE Transactions on Geoscience and Remote Sensing* **45** (12): 3894–3904.
- EVANGELISTA, P.F., EMBRECHTS, M.J. & SZYMANSKI, B.K., 2006: Taming the curse of dimensionality in kernels and novelty detection. – *Applied Soft Computing Technologies: The Challenge of Complexity*: 425–438.
- FOI, 2012: <http://www.foi.se/hsi/> (2.9.2012).
- HOFFBECK, J. & LANDGREBE, D., 1996: Covariance matrix estimation and classification with limited training data. – *IEEE Transaction on Pattern Analysis and Machine Intelligence* **18** (7): 763–767.
- JACKSON, J.E., 1991: *A User's guide to principal components*. – John Wiley and Sons.
- KAY, S.M., 1998: *Fundamentals of statistical signal processing: detection theory*. – Prentice-Hall, Upper Saddle River, NJ, USA.
- KHAZAI, S., HOMAYOUNI, S., SAFARI, A. & MOJARADI, B., 2011: Anomaly detection in hyperspectral images based on an adaptive support vector method. – *IEEE Geoscience and Remote Sensing Letters* **8** (4): 646–650.
- KEREKES, J.P., 2008: Receiver operating characteristic curve confidence intervals and regions. – *IEEE Geoscience and Remote Sensing Letters* **5** (2): 251–255.
- KWON, H. & NASRABADI, N.M., 2005: Kernel RX-algorithm: a nonlinear anomaly detector for hyperspectral imagery. – *IEEE Transactions on Geoscience and Remote Sensing* **43** (2): 388–397.
- KWON, H. & NASRABADI, N.M., 2007: A comparative analysis of kernel subspace target detectors for hyperspectral imagery. – *EURASIP Journal on Advances in Signal Processing* **2007** (1).
- MARTINEZ, W.L., MARTINEZ, A. & SOLKA, J., 2010: *Exploratory data analysis with MATLAB*. – Second Edition, CRC Press.
- MATTEOLI, S., CARNESECCHI, F., DIANI, M. & CORSINI, G., 2007: Comparative analysis of hyperspectral anomaly detection strategies on a new high spatial and spectral resolution data set. – *SPIE* **6748**.
- MATTEOLI, S., DIANI, M. & CORSINI, G., 2009: Different approaches for improved covariance matrix estimation in hyperspectral anomaly detection. – *Riunione Annuale GTTI*: 1–8.
- MATTEOLI, S., DIANI, M. & CORSINI, G., 2010: A tutorial overview of anomaly detection in hyperspectral images. – *IEEE A&E Systems Magazine* **25** (7): 5–27.
- NASRABADI, N.M., 2008: Regularization for spectral matched filter and RX anomaly detector. – *SPIE* **6966**.
- NASRABADI, N.M., 2009: Kernel subspace-based anomaly detection for hyperspectral imagery. – *Hyperspectral Image and Signal Processing: Evolution in Remote Sensing, WHISPERS '09*.
- RANNEY, K.I. & SOUMEKH, M., 2006: Hyperspectral anomaly detection within the signal subspace. – *IEEE Geoscience and Remote Sensing Letters* **3** (3): 312–316.
- REED, I.S. & YU, X., 1990: Adaptive multiple-band CFAR detection of an optical pattern with unknown spectral distribution. – *IEEE Transactions on Acoustics, Speech, and Signal Processing* **38** (10): 1760–1770.
- RIT, 2012: <http://dirsapps.cis.rit.edu/blindtest/> (2.9.2012).
- SCHÖLKOPE, B., SMOLA, A. & MULLER, K.-R., 1998: *Nonlinear component analysis as a kernel eigen-*

- value problem. – *Neural Computation* **10**: 1299–1319.
- SCHÖLKOPF, B., WILLIAMSON, R.C., SMOLA, A. & SHAWE-TAYLOR, J., 1999: SV estimation of a distribution's support. – NIPS'99.
- SCHÖLKOPF, B., PLATT, J.C., SHAWE-TAYLOR, J. & SMOLA, A., 2001: Estimating the support of a high dimensional distribution. – *Neural Computation* **13** (7): 1443–1471.
- SCHWEIZER, S.M. & MOURA, J.M.F., 2001: Efficient detection in hyperspectral imagery. – *IEEE Transactions on Geoscience and Remote Sensing* **10** (4): 584–597.
- SNYDER, D., KERÉKES, J., FAIRWEATHER, I., CRABTREE, R., SHIVE, J. & HAGER, S., 2008: Development of a web-based application to evaluate target finding algorithms. – *IEEE International Geoscience and Remote Sensing Symposium (IGARSS)* **2**: 915–918.
- TAX, D.M.J., 2001: One-class classification. – Ph.D. dissertation, Delft University of Technology.
- TAX, D.M.J. & DUIN, R.P.W., 1999: Support vector domain description. – *Pattern Recognition Letters* **20** (11): 1191–1199.
- WADSTRÖMER, N., AHLBERG, J. & SVENSSON, T., 2010: A new hyperspectral dataset and some challenges. – SHEN, S.S. & LEWIS, P.E. (eds.): *Algorithms and Technologies for Multispectral, Hyperspectral, and Ultraspectral Imagery XVI*. – SPIE **7695**.
- WILSON, T.A., 1998: Automatic target cueing of hyperspectral image data. – Ph.D. dissertation, Air Force Institute of Technology, USA.

Addresses of the authors:

Dr. SAFA KHAZAI, Prof. Dr. ABDOLREZA SAFARI & Prof. Dr. SAEID HOMAYOUNI, Department of Surveying and Geomatics Engineering, University College of Engineering, University of Tehran, PO Box 11155-4563, Tehran, Iran, Tel: +98-021-8800884, Fax: +98-21-88008837, e-mails: {khazai}{asafari}{shomayounis}@ut.ac.ir.

Prof. Dr. BARAT MOJARADI, School of Civil Engineering, Iran University of Science & Technology, Narmak, PO Box 16765-163, Tehran, Iran, Tel: +98-21-77240399 & 77240565, Fax: +98-21-77240398, e-mail: mojaradi@iust.ac.ir.

Manuskript eingereicht: Februar 2012

Angenommen: Juni 2012